Available online at www.sciencedirect.com
ScienceDirect
Polymer 49 (2008) 1853–1859
polymer
www.elsevier.com/locate/polymer

Morphological changes in poly(ε-caprolactone) in dense carbon dioxide

Erdogan Kiran*, Kun Liu, Katrina Ramsdell[1]

Department of Chemical Engineering, Virginia Tech, 132 Randolph Hall, Blacksburg, VA 24061, United States

Received 22 December 2007; received in revised form 7 February 2008; accepted 8 February 2008
Available online 14 February 2008

Abstract

Morphological changes that take place in poly(ε-caprolactone) upon exposure to carbon dioxide at high pressures have been explored as a function of pressure and temperature. SEM and DSC results point to a competition between CO_2-modulated crystallization and pressure-induced phase separation which leads to unique morphologies. At 293 K, exposure to CO_2 at pressures up to 45 MPa leads to recrystallization resulting in higher level of crystallinity and higher melting temperatures. Highest crystallinity levels along with distinct crystal morphology were observed after exposure to CO_2 at 308 K and 21 MPa. At a higher pressure at this temperature (308 K/34 MPa) polymer undergoes melting, and foaming is achieved during depressurization prior to solidification. At 323 K, the polymer is found to display unique crystal morphology with concave crystal geometry as well as porous domains. The results are discussed in terms of the crystallization and phase separation paths that are followed during exposure to CO_2 and the depressurization stages.

Keywords: Poly(ε-caprolactone); Carbon dioxide; Morphology

1. Introduction

Poly(ε-caprolactone) (PCL), $-[(CH_2)_5-COO]_n-$, is a semi-crystalline, biodegradable aliphatic polyester which is of much interest in drug delivery, tissue engineering and biomedical device applications [1–5]. It has a relatively low melting temperature in the range 323–333 K. Its glass transition temperature is reported to be at around 211 K [2]. Its blends, in particular with poly(ethylene glycol), are being explored for biomedical applications [6,7]; and its blends with other polymers such as styrene–acrylonitrile copolymers, poly(vinyl chloride), or polystyrene are under investigation in which PCL is considered as a plasticizer or used to control morphology [8–11]. Morphological features, foaming and pore formation in PCL and its blends and copolymers are of particular interest in construction of scaffolds for tissue engineering applications [12–15].

There have been several earlier studies on the solubility of CO_2 in PCL [19] and on the influence of carbon dioxide on PCL and its blends [9,20–22]. Leeke et al. [19] reported that the solubility of CO_2 reaches about 3 g CO_2/g PCL at 313 K at 200 bar, and 1.5 g CO_2/g PCL at 333 K. The plasticization effects were negligible if pressures were lower than 80 bar. Shieh and Yang [22] have reported CO_2 sorption levels at 308 K which were 4% at 8.5 MPa and 6% at 31 MPa. From the changes in the opacity of the samples, the authors deduced that at 308 K and 31 MPa, PCL must be undergoing melting, which would then undergo recrystallization upon depressurization. The extent of melting was inferred to be less at lower pressures. They proposed a heterogeneous morphology based on small angle X-ray scattering data and the endothermic shoulders that were observed in the DSC scans of the processed samples. SEM results were not reported. In a later study, the same authors reported on the morphological changes of PCL in supercritical CO_2 in the presence of poly(vinyl chloride) [9]. In the presence of PVC, the melting temperature of PCL was depressed. At a given composition, the blends were observed to exhibit lower melting temperatures following exposure to CO_2 and depressurizations, which were attributed to PCL crystals becoming thinner.

* Corresponding author.
E-mail address: ekiran@vt.edu (E. Kiran).
[1] Present address: Department of Chemical Engineering, University of Michigan, Ann Arbor, MI, United States.

0032-3861/$ - see front matter © 2008 Elsevier Ltd. All rights reserved.
doi:10.1016/j.polymer.2008.02.017

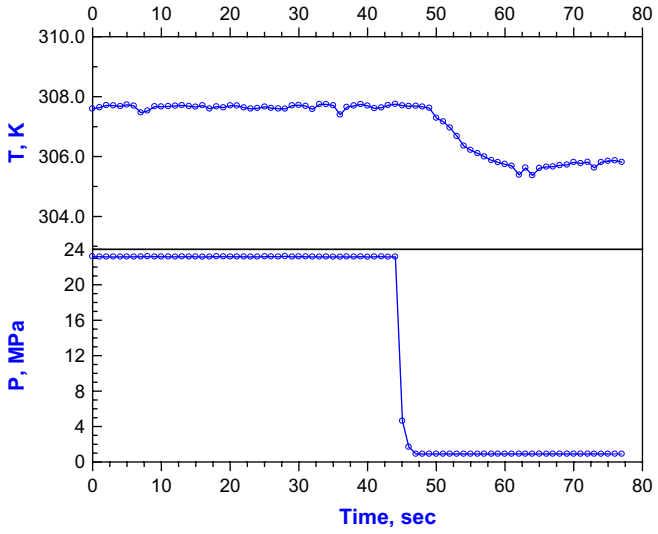

Fig. 1. Pressure and temperature change during decompression of the view cell from an initial pressure of 23 MPa to ambient pressure.

There have also been some studies on the foaming of PCL with CO_2. Xu et al. reported foaming experiments in which PCL samples were first saturated at 323 K and 10–16 MPa, which were then depressurized [21]. They reported that the pore cell size decreased when samples were saturated in the higher pressure range (14–16 MPa) compared to foaming conducted at 10 MPa. Foaming of PCL has also been explored with CO_2 and N_2 and their mixtures [20]. At 313 K, the authors reported CO_2 sorption levels of 4% at around 3 MPa and 8% at around 6 MPa, and noted the suppression of the melting temperature of PCL. They have reported foaming results for saturation pressures in the range 3–6 MPa and temperatures in the range from 300 to 308 K. The SEM results for foams obtained at around 303 K and for a sample saturated at 5.5 MPa show closed-cell morphology with relatively large pores, with cell pore diameters at around 400 μm.

We have been interested in the miscibility and phase separation of this polymer in dense fluid mixtures consisting of carbon dioxide and organic solvents such as acetone. We have recently reported on various properties of these solutions and the phase boundaries [16a,b] as a function of pressure, temperature and composition. We have also been exploring blending of PCL with glassy polymers such as poly(methyl methacrylate) to modulate its microstructural or morphological attributes [16b]. Morphological modification of polymers in dense fluids is a more recent activity in our laboratory [17,18] with implications on particle and fiber formation, and on formation of the porous materials and foams. In this paper we are presenting recent results on the unique morphological features of PCL that develop upon exposure to high pressure carbon dioxide at different pressures and temperatures.

2. Experimental

Poly(ε-caprolactone) ($M_w = 14{,}300$; $M_n = 2.3$) was obtained from Scientific Polymer Products, Inc. A Perkin–Elmer Pyris Diamond DSC unit was used for thermal characterizations. Microscopic characterizations were carried out using Leo® 1550 field emission scanning electron microscope (FESEM). For FESEM analyses, the samples were freeze-fractured and coated with a thin layer of gold.

Exposure to CO_2 and depressurizations were carried out in a variable volume view cell [17,23]. SCF/SFE grade carbon dioxide (Air Products and Chemicals) was used. The view cell is equipped with two sapphire windows for direct observations, and the changes in T, P during heating and pressurization, and during depressurization are monitored in real time. For foaming experiments, polymer samples (about 50–60 mg) were first formed into cylindrical disks (with a diameter of about 12 mm and thickness of 1 mm) using a mold and a Carver press by applying 1 ton pressure at ambient temperature. They were then exposed to CO_2 at selected pressures (21, 34, and 45 MPa) and temperatures (293, 308 and 323 K) for 30 min, and then depressurized. Typical depressurization times were 2 s and always are accompanied with a reduction in temperature. These are illustrated in Fig. 1 for a decompression from 23 MPa to ambient pressures. Samples were then removed from the view cell for further characterizations by SEM and DSC.

3. Results and discussions

3.1. SEM observations

Fig. 2a–c shows the FESEM micrographs for the fractured cross-section of the PCL disk prior to exposure to carbon dioxide at magnifications of 900, 2000 and 10,000. It is non-porous solid, and close examination reveals features that indicate presence of spherulitic domains, which are easier to observe in Fig. 2b. These are similar to the SEM micrographs reported for PCL in the literature [24].

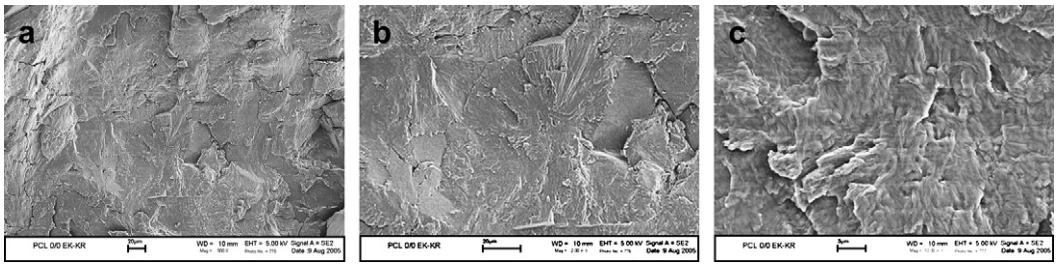

Fig. 2. SEM results of PCL prior to exposure to CO_2. Magnifications are at 900 (scale bar = 20 μm); 2000 (scale bar = 20 μm); and 10,000 (scale bar = 3 μm).

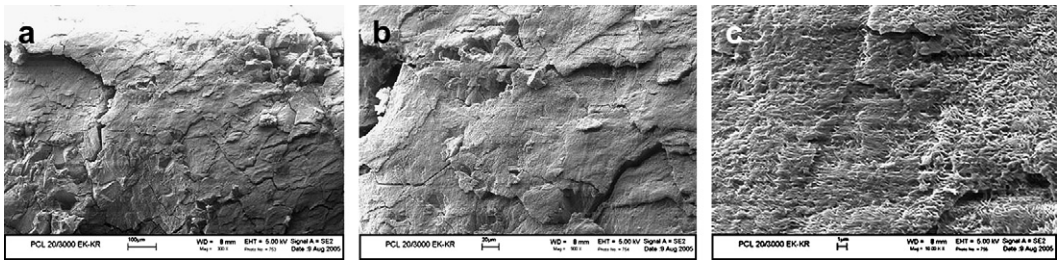

Fig. 3. SEM results of PCL after exposure to CO_2 at 293 K and 21 MPa. Magnifications are at 300 (scale bar 100 μm); 900 (scale bar = 20 μm); and 10,000 (scale bar = 1 μm).

Fig. 3a–c shows the morphology after exposure and expansion at 293 K and 21 MPa at magnifications of 300, 900 and 10,000. At high magnification, the appearance is as if there is a nano-porous morphology, but as discussed below, this is due to the crystalline lamellar growth patterns, rather than pores.

Fig. 4a–c shows the results after exposure to CO_2 at 293 K and 45 MPa. Here the micrographs demonstrate the spherulitic growth more clearly. At magnifications of 10,000 (Fig. 4b) and 20,000 (Fig. 4c), the crystal boundaries and the details of the lamellar growth on the crystal surface are distinctly displayed. Compared to ambient conditions, and exposure to CO_2 at 21 MPa, at 45 MPa it is clear that PCL undergoes recrystallization.

Fig. 5a–c shows the results of exposure at a higher temperature, 308 K and 21 MPa. Here the crystalline morphology is remarkably distinct. The SEM pictures show the three-dimensional views of the crystals with their impingement boundaries and strikingly flat surfaces that are decorated with the lamellar growth patterns. Compared to the 293 K case, recrystallization is greatly promoted at this temperature even at 21 MPa.

Fig. 6 shows the results at the same temperature (308 K) but at a higher pressure, at 34 MPa. Here the morphology is much different. PCL at this condition appears to basically melt and undergoes foaming during depressurization. A micro-porous morphology is displayed with pore sizes of about 1 μm. However, at lower magnification some elements of ''straight-edge'' morphology reminiscent of the morphologies observed in Fig. 5 are still noted.

Fig. 7 shows the morphology after exposure to CO_2 at 323 K and 34 MPa. Here a heterogeneous morphology is displayed. There appears to be spherulitic crystalline domains with a concave topography and also porous non-crystalline domains in-between.

3.2. DSC observations

The changes in the crystalline melting temperatures and the heat of melting in the samples after exposure to CO_2 were assessed by ambient pressure DSC measurements at a heating rate of 20 K/min in inert nitrogen atmosphere. Fig. 8 is a comparative plot (normalized to unit mass) of the first heating scans for the samples discussed in Figs. 2–7. Table 1 provides the melting temperatures and the heat of melting values that were evaluated from these scans.

Many of the DSC scans shown in Fig. 8 display double melting transitions. As discussed in our earlier publications, multiple melting peaks during DSC measurements are

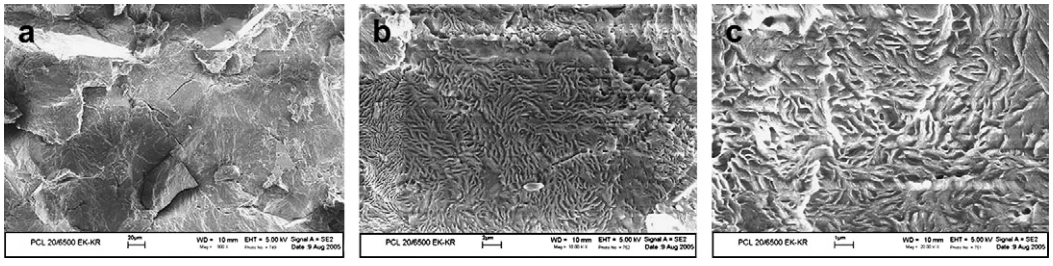

Fig. 4. SEM results of PCL after exposure to CO_2 at 293 K and 45 MPa. Magnifications are at 900 (scale bar = 20 μm); 10,000 (scale bar = 2 μm); and 20,000 (scale bar = 1 μm).

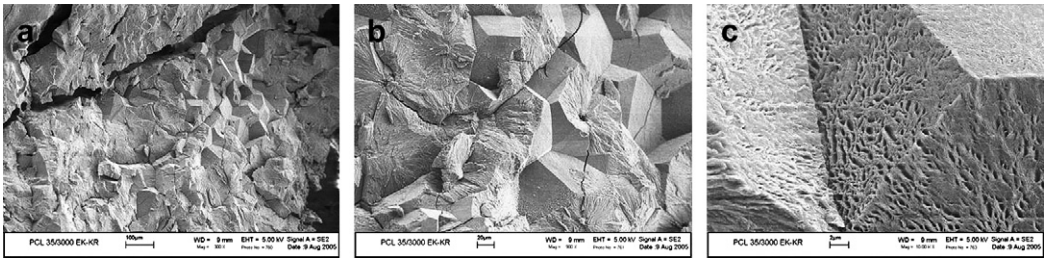

Fig. 5. SEM results of PCL after exposure to CO_2 at 308 K and 21 MPa. Magnifications are at 300 (scale bar = 100 μm); 900 (scale bar = 20 μm); and 10,000 (scale bar = 2 μm).

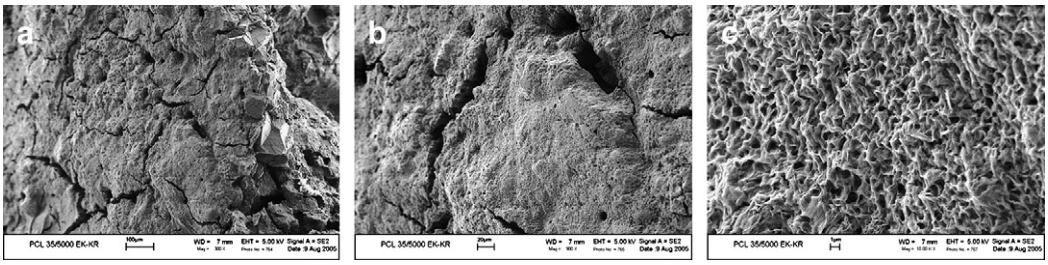

Fig. 6. SEM results of PCL after exposure to CO_2 at 308 K and 34 MPa. Magnifications are at 300 (scale bar = 100 μm); 900 (scale bar = 20 μm); and 10,000 (scale bar = 1 μm).

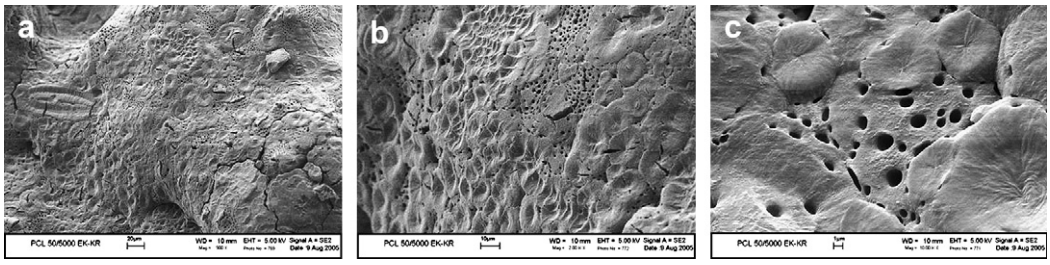

Fig. 7. SEM results of PCL after exposure to $CO_{2\ at}$ 323 K and 34 MPa. Magnifications are at 900 (scale bar = 20 μm); 2000 (scale bar = 10 μm); and 10,000 (scale bar = 1 μm).

common in crystals formed under extreme pressure in melts or crystals formed from solutions at high pressures [17]. There are several possibilities. These include (a) recrystallization of metastable crystals upon heating during which the fold length of the folded-chain crystals is altered (increased) and thus melting temperatures are shifted (to higher temperatures), (b) crystallization in the amorphous regions between the lamellae, (c) actual presence of crystals with different lamellar thicknesses, which may arise from the different crystallization kinetics and/or the different undercooling experienced during the rapid cooling or depressurization paths. In systems where the crystallization is preceded by a liquid–liquid phase separation, different crystals with different fold lengths are expected.

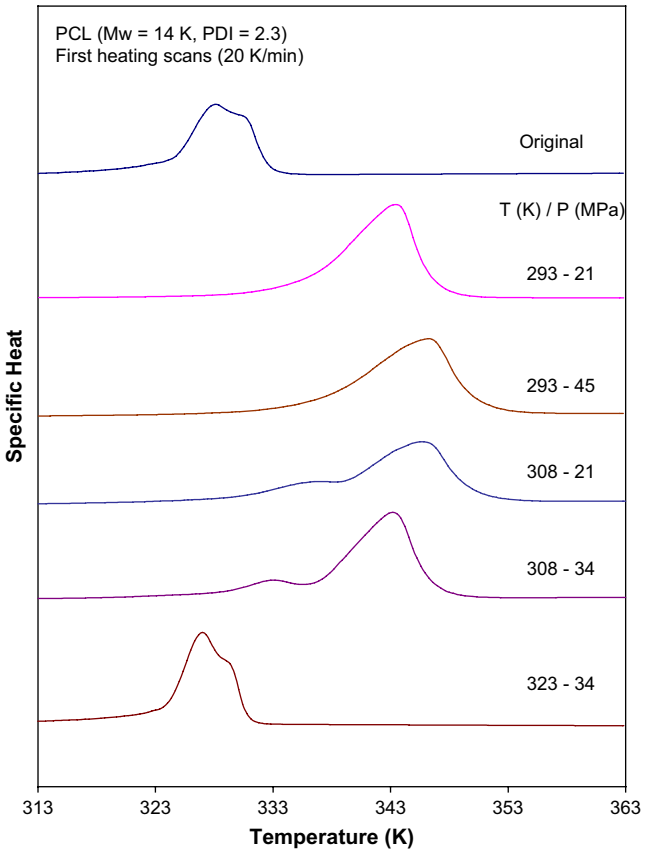

Fig. 8. DSC 1st heating scans (at 20 K/min) of PCL samples exposed to CO_2 at the indicated T (K)/P (MPa) conditions.

In the present system at 293 K, compared to the original sample, the melting temperatures are increased by about 15 K indicating increased lamellar thickness, and the heat of melting data indicate about 40% more crystallinity after exposure to CO_2 at high pressures. At 308 K, the doublet in the melting peak becomes clear, which is indicative of the heterogeneity of the crystal sizes. The lower melting temperature fractions constitute a smaller portion. Compared to treatment

Table 1
Melting temperatures and the heat of melting of PCL after exposure to carbon dioxide at various T/P conditions as determined from DSC scans with 20 K/min heating rate at ambient pressure

Processing condition		DSC tests	
T (K)	P (MPa)	T_m[a] (K)	ΔH[a] (J/g)
Original	0.1	327/329	77
293	21	343	113
293	45	346	113
308	21	335/345	104
308	34	333/343	110
323	34	327/329	79

[a] For those scans displaying doublet melting peaks the peak temperatures are indicated, and the heat of melting corresponds to total heat of melting.

at 293 K, here the melting temperature shifts to a lower temperature which becomes more accentuated at higher pressures. Heat of melting is also reduced. After exposure to CO_2 at 323 K at high pressure, the DSC data show a thermal behavior very similar to that of the original PCL. Here, it is clear that the polymer undergoes complete melting in the presence of carbon dioxide, and during depressurization, the dynamics of the temperature reduction and the reduction in the amount of dissolved CO_2 do not lead to immediate crystallization, and the crystallization appears to have proceeded as if it would be from melt at ambient pressures. Here, the thinner lamellar fractions with a lower melting temperature appear to be the more dominant fraction, which is in contrast to the samples that were treated at lower temperatures.

4. Discussion

It should be noted that the DSC results support the SEM results. The high melting temperatures are observed for the samples prepared at 293 K and 45 MPa (Fig. 4) or at 308 K and 21 MPa (Fig. 5). As shown by the SEM results, these samples indeed display the distinct crystalline domains. The lowest T_m is obtained for samples that were exposed to CO_2 at 323 K (Fig. 7). This is consistent with the comparatively greater expansion with this sample and the formation of the pores in the non-crystalline domains as shown in Fig. 7. Lowering of T_m promotes the possibility for porous structure formation, which is also observed in samples prepared at 308 K and 34 MPa (Fig. 6). The comparative assessment of the SEM and DSC data shows that at 293 K, the process is recrystallization that is promoted basically by the enhanced chain mobility that would come about with sorption of CO_2 in the polymer. The polymer does not undergo complete melting at these conditions. The amount of CO_2 dissolved does not bring the melting temperature below 293 K. During depressurization the system simply crosses the solid–fluid phase boundary (crystallization). At 308 K and 21 MPa, the crystal thickening process is further facilitated, and it appears that depression of the crystalline melting temperature of the original PCL with the level of CO_2 incorporation in the polymer at this T/P may have brought it close to 308 K. At 323 K, it is clear that the polymer melts, and the system is a fluid–liquid mixture, which then undergoes solid–fluid phase separation upon depressurization. The multiple melting transitions with higher amount of the fraction with lower melting temperature indicate that the system undergoes a liquid–liquid phase separation first upon pressure reduction, leading to a polymer-rich and a polymer-lean phase. The crystallization that follows in each phase leads to the crystals with different lamellar thicknesses and melting temperatures. In this context, the DSC data for the experiments at 308 K and the appearance of a shoulder at 21 MPa which becomes a small distinguishable melting peak at 34 MPa are also suggestive of crossing the L–L boundary first, but at that temperature the system immediately afterwards appears to be crossing the solid–fluid boundary forming the crystals.

These observations demonstrate the importance of the phase separation path in polymer–fluid systems. We have previously shown this with crystallization of polyethylene [17]. Fig. 9 is a cartoon of temperature–composition phase diagram in which liquid–liquid (shaded areas) and also the fluid–solid (crystallization, T_c) phase boundaries are depicted. In a dense fluid increasing the pressure usually makes the fluid a better solvent. It shifts the LCST to significantly higher temperatures, the UCST to somewhat lower temperatures. Crystallization temperature is lowered with fluid sorption, and shifts the crystallization temperature to lower temperatures. At a given composition x_1, increasing the pressure would increase the equilibrium crystallization temperature from T_c, P_1 to T_c, P_2. When the initial polymer (IP) is exposed to the fluid at T_1, fluid dissolves in the polymer, and the composition shifts to x_1. The degree of undercooling the polymer now experiences changes from "a" to "b" (depicted by arrows), upon which the lamellar thickening in the existing crystalline domains may be promoted. As long as the prevailing T/P conditions do not take the polymer above the T_c curve, these transformations occur in the solid polymer phase that is in equilibrium with the fluid. During depressurization, the dissolved fluid escapes from the polymer matrix, the temperature is further reduced, and the concentration moves towards the 100% polymer case. The end result is a polymer with crystals with larger lamellar thickness and thus of higher melting temperatures. This is what is observed in systems at 293 K and at for example 21 MPa. When the pressure is increased to a higher pressure like $P = 45$ MPa, the degree of incorporation

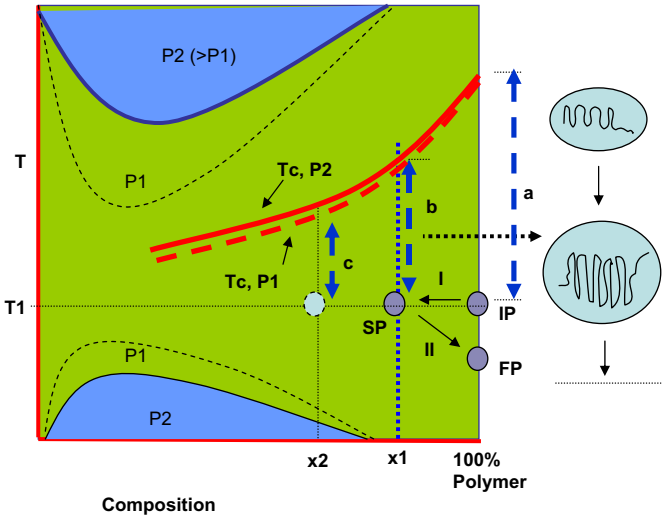

Fig. 9. Crystal modification of initial polymer (IP) with fluid sorption at high pressure (path I) when the solvent + polymer (SP) system remains below the equilibrium crystallization curve T_c. The polymer does not melt. Because of the increased chain mobility and the system getting closer to the melting temperature (indicated by double-headed arrows), lamellar thickening is promoted. This is locked-in during depressurization (Path II along which temperature is further decreased and the polymer concentration increases with fluid escaping from the matrix). At the end of depressurization, the final polymer (FP) displays a higher melting temperature and greater level of crystallinity than the original polymer. Dark shaded areas represent the liquid–liquid two-phase regions at pressure P2, which shift at pressure P1 to new boundaries shown with the dashed curves.

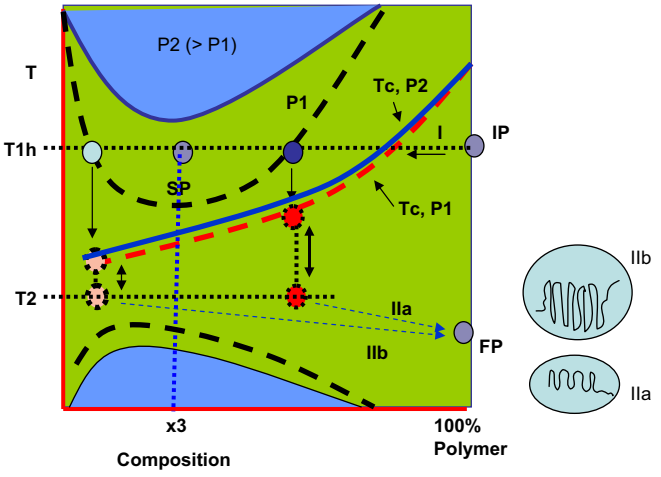

Fig. 10. Crystal modification with fluid sorption at a higher temperature (T_{1h}) and high pressure (P_2) upon which the initial polymer (IP) melts and forms a homogeneous one-phase solution of solvent + melt (SP). During depressurization (for example to P_1), the initially homogeneous system enters two-phase region and first undergoes liquid–liquid phase separation forming a polymer-lean and a polymer-rich phase. Crystal formation and modifications proceed upon further cooling (for example to T_2) and final depressurization (Paths IIa and b) as the fluid escapes from the polymer-rich and polymer-lean phases. During the final decompression stage, the crystallization curve moves upward and temperature is further reduced. Different degrees of undercooling and the chain mobility experienced in the two-phases then lead to different crystalline domains with different lamellar thicknesses, and as a consequence, the final polymer (FP) displays double melting points.

of CO_2 in the polymer is increased, moving the position of the polymer concentration to x_2 where T_c is at a lower temperature compared to the condition at x_1, and the degree of undercooling (indicated by the arrow c) that the polymer experiences becomes even smaller. This further promotes the crystal rearrangement, as has been suggested by the SEM and DSC results. At 308 K and 21 MPa, the systems still remain below the polymers' equilibrium crystallization T at the level of fluid sorption at this T/P conditions, and the process promotes the crystal rearrangement in the solid state.

Fig. 10 is a cartoon depicting the process at a higher T (T_{1h}) like 323 K or at 308 K but at a higher pressure (P_2) (i.e., 34 MPa). Here the initial polymer (IP) upon sorption of the fluid in the polymer moves to composition x_3. At this composition, and the temperature/pressure, the system is above the equilibrium crystallization temperature (above T_c, P_2), that is, it melts and forms a homogeneous solution. This depends on the location of the LCST or UCST in the system, which we have not determined, and there is no direct experimental information in the literature as to PCL + CO_2 system having an LSCT- or UCST-like phase behavior. In PCL + CO_2 - + acetone, the behavior has been previously shown to be LCST-type [15]. The discussion that follows is presented for the LCST case, but descriptions can be generated equally well for the UCST situation. It should be pointed out that in ternary systems as the CO_2 amount is increased there is usually a switchover from LCST to UCST type behavior [25] and thus PCL + CO_2 system could well be a UCST-type system. Blends of PCL with polystyrene in the absence of solvents are reported to show UCST [26,27] whereas its blends with SAN show LCST [28].

In Fig. 10, during depressurization, the solvent strength is reduced and LCST moves to lower temperature, and the system undergoes a liquid–liquid phase separation. Upon further cooling to T_2 and crossing the S–F boundary, the polymer-lean and polymer-rich phases being at different distance from the equilibrium crystallization curve experience different degrees of undercooling. During further decompression, as the fluid escapes from the polymer, the melting curve moves to even higher temperatures. Two different crystal size domains and double melting peaks are indeed observed in experiments conducted at 308 K at higher pressures and at 323 K.

The present study confirms the deductions that were made in the literature from X-ray data that PCL melts when exposed to CO_2 at 308 K and 31 MPa [9]. In a recent publication [29], melting temperatures of PCL in the presence of CO_2 has been reported at pressures in the range from 0.1 to 27.6 MPa. At 27.6 MPa, T_m is reported to be 307.2 K. The lamellar growth patterns in Figs. 3 and 4 display some orientational changes. Periodic twisting of lamellar crystals is reported in the literature to occur in PCL crystals formed in solution-cast films [30]. Ring-banded spherulites are reported to arise from nonlinear diffusion during growth. Edge-on lamellar growth patterns have also been observed in the spherulites formed in blends of PCL with poly(ethylene oxide) [31] where some of the unique morphologies were attributed to confinement effects. It should be noted that crystallization of a different polymer (high density polyethylene) in gas-assisted injection molding that was reported recently displays lamellar growth patterns that show strikingly similar attributes to the lamellar edge patterns displayed in Fig. 4. Here the authors attributed the orientational features to shear effects [32]. In Fig. 7, SEM results display a concave geometry for the PCL crystals. These lily-like spherulitic structures have been reported in crystallization of PCL and its blends with polystyrene prepared from 5 wt% solutions in THF where the dynamics of L–L phase separation in the blend and the crystallization of PCL influence the final morphology [26].

It should be noted that Fig. 5 displays a set of rare micrographs which show the three-dimensional growth of the spherulitic crystals with sharp impingement planes for poly(ε-caprolactone) – and for that matter, possibly for any polymer. Essentially all crystallization studies in the literature show micrographs for spherulitic crystals that are formed in thin films or confined geometries where the spherulitic growth and the impingement boundaries appear as lines. For example in a study of poly(ε-caprolactone) crystal growth in ultrathin films (ca. 200 nm) the AFM height images show distinct boundaries that would be very similar to what a cross-section of the three-dimensional morphologies shown in Fig. 5 would be [33]. Sharp boundaries of impingent spherulites have been reported also, again in thin films (about 40 μm), for isotactic polystyrene [34]. These authors point out that during spherulitic crystallization, the crystallization front rejects the noncrystallizable fractions (such as short chains or impurities), leading to boundaries between adjacent spherulites that

represent a high concentration of non-crystallizable materials. They have further inferred that in-between the spherulitic domains there is an amorphous region which appears as darker line in the AFM images. In the present SEM studies, the samples were prepared by fracturing in liquid nitrogen, during which some of the spherulitic domains appear to have been dislodged from their positions and have fallen off (which could be facilitated if indeed an in-between layer between the spherulitic domains existed) exposing the impingement planes, with the edge-on lamellar growth patterns remaining visible. What is remarkable is the clear individual identity of the crystalline domains without any visible tie chains between the neighboring spherulitic entities.

5. Conclusions

The present results demonstrate the significance of the path followed in the modifications of PCL in dense CO_2. The results show that recrystallization of PCL is promoted in carbon dioxide at temperatures and pressures where chain mobility is enhanced while the system remains below the crystalline melting temperature. Foaming is promoted at higher temperatures and pressures where the dissolution of CO_2 in the polymer leads to melting of PCL. Final morphology is influenced by the combined effect of recrystallization and phase separation processes.

References

[1] Martina M, Humacher DW. Polym Int 2007;56:145.
[2] Armani DK, Liu C. J Micromech Microeng 2000;10:80.
[3] Ashammakhi N, Ndreu A, Yang Y, Ylikauppila H, Nikkola L, Hasirci V. J Craniofacial Surg 2007;18:1.
[4] Elvira C, Fanovich A, Fernandez M, Fraile J, Roman JS, Domingo C. J Controlled Release 2004;99:231.
[5] Wang Y, Chang HI, Wertheim DF, Jones AS, Jackson C, Coombes AJA. Biomaterials 2007;28:4619.
[6] Chuang WT, Shih KS, Hong PD. J Polym Res 2005;12:197.
[7] Quinn TP, Oreskovic TL, Landis FA, Washburn NR. J Biomed Mater Res Part B Appl Biomater 2007;82(1):205.
[8] Madbouly SA, Ougizawa T. Macromol Chem Phys 2004;205:1923.
[9] Shieh YT, Yang HS. J Polym Sci Part B Polym Phys 2006;44:85.
[10] Sarazin P, Favis BD. Polymer 2005;46:5966.
[11] Eastmond GC. Adv Polym Sci 2000;149:59.
[12] Maio ED, Iannace S, Marrazzo C, Narkis N, Nicolais L. Macromol Symp 2005;228:219.
[13] Jenkins MJ, Harrison KL, Silva MMCG, Whitaker MJ, Shakesheff KM, Howdle SM. Eur Polym J 2006;42:3145.
[14] Zhou J, Villaroya S, Wang W, Wyatt MF, Duxbury CJ, Thurecht KJ, et al. Macromolecules 2007;40:2276 [additions/corrections];
Zhou J, Villaroya S, Wang W, Wyatt MF, Duxbury CJ, Thurecht KJ, et al. Macromolecules 2006;39:5352.
[15] Peraglio M, Gremeillard L, Chevalier J, Chazeau L, Gauthier C, Hammaide T. J Eur Ceram Soc 2007;27:2679.
[16] (a) Liu K, Kiran E. Polymer 2007;48:5612;
(b) Liu K, Kiran E. Polymer 2008;49:1555.
[17] (a) Zhang W, Kiran E. J Supercrit Fluids 2006;38:406;
(b) Upper G, Beckel D, Zhang W, Sohn S, Liu K, Kiran E. Ind Eng Chem Res 2005;45:1478.
[18] Fang J, Kiran E. J Supercrit Fluids 2006;38:132.
[19] Leeke GA, Cai JG, Jenkins M. J Chem Eng Data 2006;51:1877.
[20] Di Maio E, Mensitieri G, Iannace S, Nicolais L, Li W, Flumerfelt RW. Polym Eng Sci 2005;45:432.
[21] Xu Q, Ren X, Chang Y, Wang J, Yu L, Dean K. J Appl Polym Sci 2004; 94:593.
[22] Shieh YT, Yang HS. J Supercrit Fluids 2005;33:183.
[23] Bayraktar Z, Kiran E. J Supercrit Fluids 2008;44:48.
[24] Aroguz AA, Engin HH, Baysal BM. Eur Polym J 2007;43:403.
[25] Kiran E. In: Kiran E, Debenedetti PG, Peters CJ, editors. Supercritical fluids: fundamentals and applications. Dordrecht, The Netherlands: Kluwer Academic Publishers; 2000. p. 167–92.
[26] Shabana HM, Olley RH, Bassett DC, Jungnickel BJ. Polymer 2000;41: 5513.
[27] Nojima S, Satoh K, Ashida T. Macromolecules 1991;24:942.
[28] Svoboda P, Keyzlarova L, Saha P, Rybnikar F, Chiba T, Inoue T. Polymer 1999:1459.
[29] Lian Z, Epstein SA, Blenk CW, Shine AD. J Supercrit Fluids 2006;39: 107.
[30] Wang Z, Hu Z, Chen Y, Gong Y, Huang H, He T. Macromolecules 2007;40:4381.
[31] Hou WM, Zhou JJ, Gan ZH, Shi AC, Chan CM, Li L. Polymer 2007;48: 4926.
[32] Zheng GQ, Huang L, Yang W, Yang B, Yang MB, Li Q, et al. Polymer 2007;48:5486.
[33] Mareau VH, Prude'homme RE. Macromolecules 2005;38:398.
[34] Liu T, Ma K, Liu Z, He C, Chung TS. J Appl Polym Sci 2002;86: 422.